An average atom code for warm matter: application to aluminum and uranium

2009 J. Phys.: Condens. Matter 21 095409

(http://iopscience.iop.org/0953-8984/21/9/095409)

J. Phys.: Condens. Matter **21** (2009) 095409 (8pp) doi:10.1088/0953-8984/21/9/095409

An average atom code for warm matter: application to aluminum and uranium

Michel Pénicaud

Commissariat à l'Energie Atomique, DAM-Île de France, BP 12, F-91680 Bruyères le Châtel, France

E-mail: michel.penicaud@gmail.com

Received 29 September 2008, in final form 8 January 2009
Published 4 February 2009
Online at stacks.iop.org/JPhysCM/21/095409

Abstract

In astrophysics and in other sciences there is sometimes a need for information about the properties of matter, particularly equations of state, in extreme conditions of pressure and temperature. Global equation of state models, which represent solid, fluid and plasma states, typically consist of three parts: the cold curve, the ion-thermal contribution and the electron-thermal contribution. For the calculation of the latest part we present here an average atom embedded in a jellium code. We employ Liberman's relativistic and quantum model of matter which is a significant advance in complexity beyond the commonly used Thomas–Fermi model. We have applied specific algorithms to deal with the highly oscillatory nature of the free wavefunctions at high temperatures and to capture resonances which form in the continuum when bound states are destroyed by pressure ionization. Also we use massive parallel computing to treat the huge number of free wavefunctions at high temperatures (up to 10^9 K). Densities of states of resonant states are shown for uranium. With our code, which we have called Paradisio, we obtain tables of electron-thermal entropies from which free energies and pressures are derived. Our results are compared with those calculated in the Thomas–Fermi approximation and with available experiments. In aluminum, with our quantum code, a shell structure appears on the Hugoniot and a first-order metallic–nonmetallic transition is created at low densities and temperatures.

(Some figures in this article are in colour only in the electronic version)

1. Introduction

The jellium is a uniform electron gas with a positive charge background. We consider systems where a single atom is embedded in a jellium. This model can be useful for condensed matter and plasmas. It could allow us to calculate thermodynamic quantities (energy, pressure, entropy, etc) and radiative properties (energy levels, matrix elements, etc).

We are particularly interested here in the determination of global equations of state (EOS). They typically consist of three parts:

$$\begin{aligned} P_t(\rho, T) &= P_c(\rho) + P_i(\rho, T) + P_e(\rho, T) \\ E_t(\rho, T) &= E_c(\rho) + E_i(\rho, T) + E_e(\rho, T), \end{aligned} \tag{1}$$

where P_t and E_t are the total pressure and energy relative to the density ρ and the temperature T. P_c and E_c are the electronic contributions at 0 K (cold curve). P_i and E_i are the thermal ionic contributions. P_e and E_e are the thermal electronic terms that will be obtained from entropy S_e tables calculated with the mean atom embedded in a jellium model of Liberman [1] in a new implementation, the Paradisio code.

The original code of Liberman, Inferno, employs two approximations to calculate the charge density of continuum electrons to reduce the cost of computation. First Thomas–Fermi (TF) is used above 10^7 K which introduces some loss of accuracy in this region. Second all continuum waves are approximated in terms of a small set of basis functions; unfortunately for this reason Inferno results become unreliable in the low-density limit [2]. In the same spirit of the Purgatorio code [2], but with different numerical procedures, we have created the Paradisio code to obtain the thermal electronic terms from a few K to billions K and densities ranging from essentially isolated ion conditions to 10^5 g cm^{-3} in uranium. In Paradisio bound and free electrons will be treated equivalently in a fully relativistic and quantum manner. We have applied

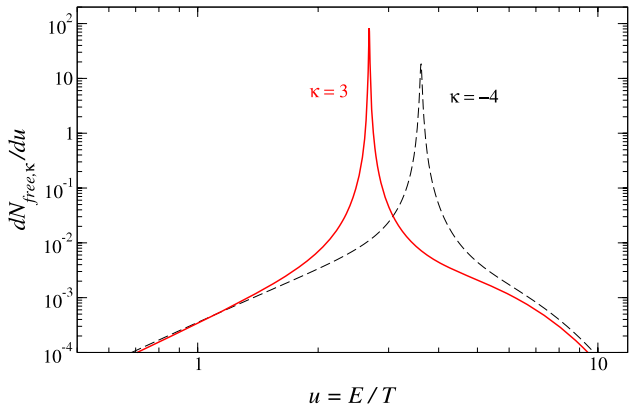

Figure 1. Density of free electrons of resonant states at 4.2 g cm^{-3} and 10^4 K for U.

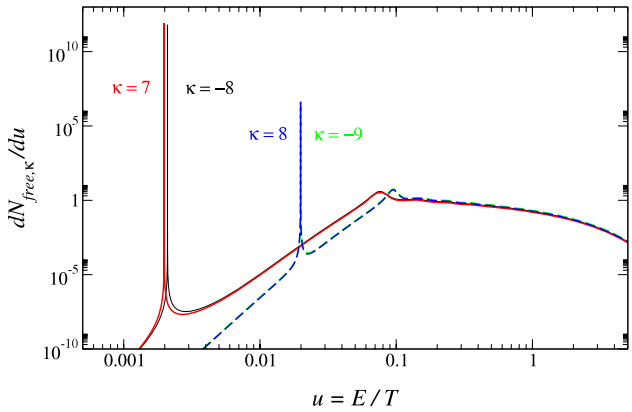

Figure 2. Density of free electrons of resonant states at 4.2 g cm^{-3} and 5.5×10^6 K for U.

specific algorithms to deal with the highly oscillatory nature of the free wavefunctions at high temperatures and to capture resonances which form in the continuum when bound states are destroyed by pressure ionization. Also we use massive parallel computing to treat the huge number of free wavefunctions at high temperatures.

2. Theory and numerical methods

The theoretical model is presented in [1]. We have chosen model A of the two choices offered by Liberman. All the quantities of interest for the atom are calculated inside the atomic sphere of radius R which keeps it apart from the surrounding electron gas.

The electrical neutrality of the atomic sphere implies that it must contain Z (atomic number) electrons. By the relation $Z = N_{\text{bound}} + N_{\text{free}}$ we obtain the chemical potential μ because the number of bound electrons is

$$N_{\text{bound}} = \sum_{\kappa,n} X_\kappa(E_n)\, D_{\text{F}}(E_n, \mu) \tag{2}$$

and the number of free electrons is

$$N_{\text{free}} = \sum_{\kappa} \int_0^\infty X_\kappa(E_k)\, D_{\text{F}}(E_k, \mu)\, \mathrm{d}E_k \tag{3}$$

κ is the Dirac quantum number connected to the angular quantum number l by $\kappa < 0\ l = -(\kappa + 1)$ and then $\kappa > 0\ l = \kappa$. For each κ, the E_n are the finite number of bound energies, the E_k are the free energies continuum which are connected to the wavevector k by the relations (4), where c is the velocity of light:

$$\begin{aligned} E_k &= c^2(\sqrt{1 + k^2/c^2} - 1) \\ k &= \sqrt{2E_k(1 + E_k/2c^2)} \end{aligned} \tag{4}$$

D_{F} is the Fermi distribution:

$$D_{\text{F}}(E, \mu) = \{1 + \exp[(E - \mu)/T]\}^{-1} \tag{5}$$

and

$$X_\kappa(E) = 2\,|\kappa| \int_0^R [g_\kappa^2(E, r) + f_\kappa^2(E, r)] r^2\, \mathrm{d}r, \tag{6}$$

where g_κ and f_κ are, respectively, the major and minor components of the radial Dirac equation.

Once we have obtained μ we can obtain the electronic density inside the atomic sphere $\rho_{\text{e}}(r) = \rho_{\text{bound}}(r) + \rho_{\text{free}}(r)$ by expressions similar to (2), (3) and (6) but without the r integration. We obtain also the electronic density in the surrounding electron gas. Then a new potential $V(r)$ can be determined and iterated to self-consistency [1]. We generally use for the starting potential the one calculated for a close temperature or density, otherwise at high temperature or high density the TF potential.

The electronic entropy $S_{\text{e}} = S_{\text{bound}} + S_{\text{free}}$ will be obtained from the formulae relative to electrons interacting through a mean field [1]. The expressions of S_{bound} and S_{free} are similar to (2) and (3) with the replacement of D_{F} by

$$F(D_{\text{F}}) = D_{\text{F}} \ln(D_{\text{F}}) + (1 - D_{\text{F}}) \ln(1 - D_{\text{F}}). \tag{7}$$

Strong numerical problems appear to calculate the continuum spectra. First, most atoms will have resonances in the continuum, and second, at high temperature (until 10^9 K) there is a huge number of highly oscillatory free wavefunctions and we have to find a way to calculate N_{free} (3).

For negative energies there are only a finite number of solutions E_n of the Dirac equation. For each κ value, we find them on a logarithmic grid, but sometimes we also find solutions for small positive energies, indicative that we shall have resonances in the continuum for this κ, κ_R. In that case, the resonance will be detected in the continuum and the maximum determined by finding the cancellation of the logarithmic derivative of the function $X_\kappa(E_k)$ (6). Then points will be added for this κ_R in the original logarithmic grid in energies of the continuum to describe the resonance correctly.

With the relation (8) we define a function which is a free electron density:

$$\frac{\mathrm{d}N_{\text{free},\kappa}}{\mathrm{d}u} = X_\kappa(E)\, D_{\text{F}}(E, \mu)\, T, \tag{8}$$

where $u = E/T$.

In figures 1 and 2 the function (8) is shown in cases with resonances, for example uranium.

For the calculation of $N_{\rm free}$ (3) we use different procedures according to the value of the chemical potential μ which gives the shape of the Fermi distribution $D_{\rm F}$. The procedures are similar for the calculations of $\rho_{\rm free}(r)$ and $S_{\rm free}$.

In the usual regime (μ/T less than 250) $D_{\rm F}$ is far from the step function. We split (3) into two parts $N_{\rm free} = N_{{\rm free},0} + N_{{\rm free},i}$ where

$$N_{{\rm free},0} = \sum_{\kappa} \int_0^{E_{\rm m}} X_\kappa(E)\, D_{\rm F}(E,\mu)\, {\rm d}E \tag{9}$$

and

$$N_{{\rm free},i} = \sum_{\kappa} \int_{E_{\rm m}}^{\infty} X_\kappa(E)\, \exp[-(E-\mu)/T]\, {\rm d}E. \tag{10}$$

For $E_{\rm m}$ we have found that we can take

$$E_{\rm m} = \max(0, \mu + 10\,T). \tag{11}$$

With that value $D_{\rm F}$ becomes, for $E \geqslant E_{\rm m}$, the classical Boltzmann distribution which behaves like an exponential tail. The integration in (10) can be made with the Gauss–Laguerre quadrature formulae. Furthermore in (10) we can assume that $X_\kappa(E)$ can be approximated by the ideal wavefunctions of an electron gas, then

$$\begin{aligned} g_\kappa &= k\sqrt{\frac{k}{\pi E}}\, j_l(kr) \\ f_\kappa &= k\sqrt{\frac{k}{\pi E}}\, s_\kappa \frac{E}{kc}\, j_{\bar{l}}(kr), \end{aligned} \tag{12}$$

where

$$\begin{array}{llll} \kappa < 0 & l = -(\kappa+1) & \bar{l} = l+1 & s_\kappa = -1 \\ \kappa > 0 & l = \kappa & \bar{l} = l-1 & s_\kappa = +1 \end{array} \tag{13}$$

and the j_l are the spherical Bessel functions of the first kind [3].

With the Bessel function identity:

$$\sum_{l=0}^{\infty} (2l+1)\, j_l^2(kr) = 1 \tag{14}$$

we obtain finally

$$X_\kappa(E) = \frac{(1+E/c^2)}{\pi^2 k} k^2 \left(\frac{4}{3}\pi R^3\right) \tag{15}$$

and then $N_{{\rm free},i}$.

Unless at small densities, at high or very low temperatures, where $E_{\rm m} = 0$ and then $N_{{\rm free},0} = 0$, we need to calculate (9).

The integral in energies in $N_{{\rm free},0}$ is done on a original logarithmic grid where points can be added if there are resonances. Usually, the summation on κ in (9) practically converges for the maximum value $\kappa_{\rm m}$ (associated to $l_{\rm m}$ by (13)); $l_{\rm m} \sim k_{\rm m} R$, where $k_{\rm m}$ is related to $E_{\rm m}$ by (4). At high temperature we can have high values of $k_{\rm m}$ and then the radial Dirac functions are very oscillatory (figure 3) because they are adjusted on the atomic sphere, with the α parameter, to the solutions outside the sphere, i.e. for the major component:

$$g_\kappa = \frac{k}{\sqrt{1+\alpha^2}}\sqrt{\frac{k}{\pi E}}\,[j_l(kr) + \alpha\, y_l(kr)] \tag{16}$$

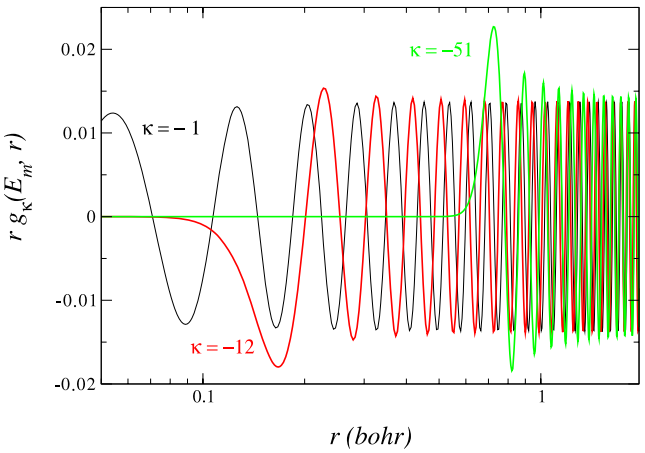

Figure 3. Oscillations of free wavefunctions for some angular momentum (κ) and for the maximum energy $E_{\rm m}$ at 85.46 g cm^{-3} and 2.69×10^8 K for U.

j_l and y_l are the spherical Bessel functions of first and second kind [3]. For large values of kr they behave like

$$\begin{aligned} j_l &\to \frac{1}{kr}\sin(kr - l\pi/2) \\ y_l &\to \frac{1}{kr}\cos(kr - l\pi/2). \end{aligned} \tag{17}$$

Then a minimum value of the period of radial oscillations of our free wavefunctions will be

$$pri = 2\pi/k_{\rm m}. \tag{18}$$

For a good description of the free wavefunctions, we will take a minimum of 25 points per *pri*. This implies that we use the variable

$$x = \ln(r) + r^2 \tag{19}$$

instead of the variable

$$x = \ln(r) \tag{20}$$

taken for bound wavefunctions, to not have too many radial points when *pri* is small. In every case we take a minimum number of points on the free radial grid always greater than or equal to the number of points on the bound radial grid.

Because we have two radial grids, we need to interpolate twice on a loop of the self-consistent process. This can be done easily. We take our potential $V(r)$ from the grid of bound wavefunctions; we interpolate it to solve the Dirac equations of the free wavefunctions. We also need to interpolate the electronic density of the free electrons to solve the Poisson equation on the simpler grid of the bound electrons.

We have found this way simpler than the phase-amplitude method used in [2] to cope with the sometimes highly oscillatory free wavefunctions.

Converged values of the electron density and its bound and continuum components are illustrated in figure 4 for U.

We also use massive parallel computing to calculate in parallel, for each κ, the free wavefunctions g_κ and f_κ.

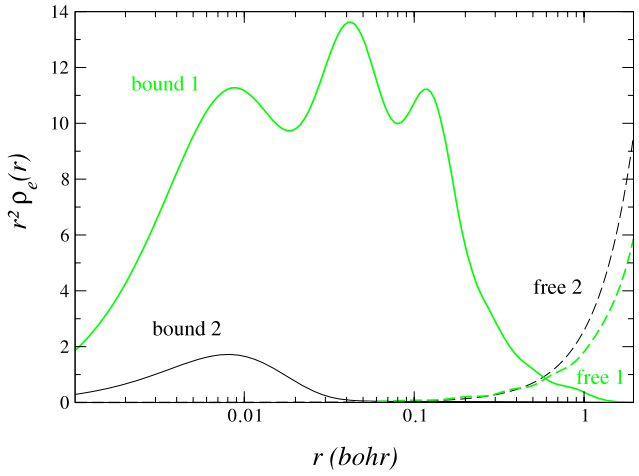

Figure 4. Radial electronic densities of bound and free electrons at 85.46 g cm^{-3} and temperatures 1.34×10^7 (1) and 2.69×10^8 K (2) for U.

In the regime where μ/T is greater than 250, D_F is close to the step function, then $N_{\text{free},i} \approx 0$ (10). To have enough points in the energy grid in the space where the variation of D_F is strong, we split the integral into (3) this way:

$$N_{\text{free}} = N_{\text{free,c}} + N_{\text{free,v}}$$

$$N_{\text{free,c}} = \sum_\kappa \int_0^{\mu-25T} X_\kappa(E) D_F(E,\mu)\,\mathrm{d}E \qquad (21)$$

$$N_{\text{free,v}} = \sum_\kappa \int_{\mu-25T}^{\mu+25T} X_\kappa(E) D_F(E,\mu)\,\mathrm{d}E. \qquad (22)$$

We take a constant number of energy points to integrate (22). The values of the function $X_\kappa(E)$ are interpolated from the initial energy grid on these points.

The procedures are similar for the calculations of $\rho_{\text{free}}(r)$ and S_{free}. This is essential to obtain $S_{\text{free}} = S_{\text{free,c}} + S_{\text{free,v}}$ because when D_F is close to the step function we have $F(D_F) \approx 0$ (7) and $S_{\text{free,c}} \approx 0$.

3. Equation of state for uranium

We have built a global EOS for U. The three parts of (1) have been assembled with the help of the Panda code [4].

3.1. Thermal electronic terms

From entropy S_e tables calculated with Paradisio, Panda gives us the other thermal electronic thermodynamic quantities P_e and E_e. We calculate first the free energy F_e:

$$F_e(\rho,T) = -\int_0^T S_e(\rho,T')\,\mathrm{d}T' \qquad (23)$$

$$E_e(\rho,T) = F_e(\rho,T) + TS_e(\rho,T) \qquad (24)$$

$$P_e(\rho,T) = \rho^2 \frac{\partial F_e(\rho,T)}{\partial \rho}. \qquad (25)$$

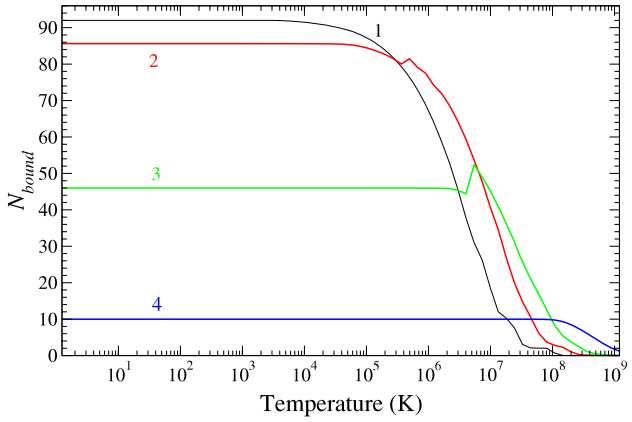

Figure 5. Number of bound electrons N_{bound} versus temperature for U for isochores 0.01 (1), 19 (2), 811 (3) and 1.2×10^5 g cm^{-3} (4).

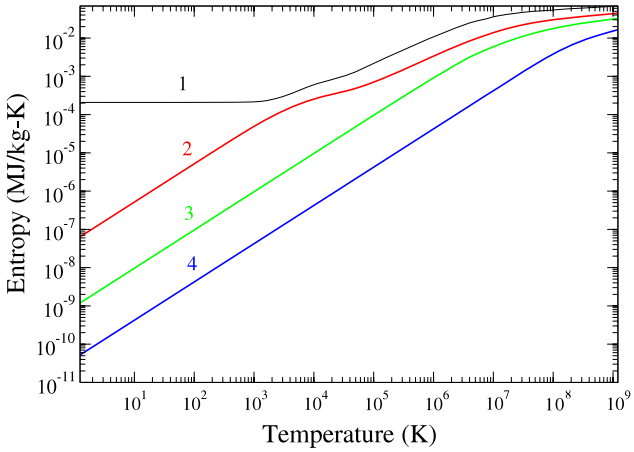

Figure 6. Entropy S_e versus temperature for U for isochores 0.01 (1), 19 (2), 811 (3) and 1.2×10^5 g cm^{-3} (4).

The entropies are calculated on a logarithmic grid in density and temperature and some isochores are shown in figure 6. In figure 5 we have plotted the corresponding isochores for the number of bound electrons N_{bound}.

We can see a peak for 811 g cm^{-3} in figure 5 which corresponds to the passing into the continuum of states $4f_{5/2}$ and $4f_{7/2}$ where they have become resonances. Therefore there is no discontinuity on the corresponding entropy isochore. The small peak for the normal density 19.07 g cm^{-3} corresponds to the passing of states $5f_{5/2}$ and $5f_{7/2}$ into the continuum. At higher temperature the bound states are less populated so their passing into the continuum is less visible.

In figure 7 a comparison is done for the normal density $\rho_0 = 19.07$ g cm^{-3} between entropies calculated by Paradisio or TF. Mainly, Paradisio entropies are greater than the TF ones for temperatures lower than 10^5 K. For $\rho < \rho_0$ the gap between TF and Paradisio is greater, it is smaller for $\rho > \rho_0$.

3.2. Thermal ionic terms

We have obtained them from the Panda code [4].

For this study we have used a simple model which interpolates between the Debye model, at low temperatures or

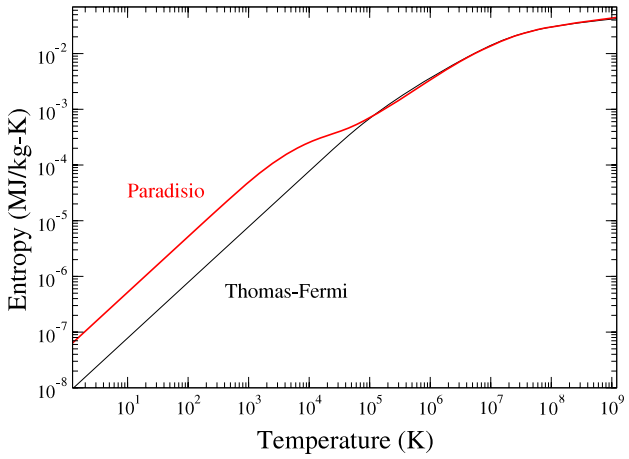

Figure 7. Comparison of entropies S_e calculated by Paradisio or TF at the normal density 19.07 g cm^{-3} for U.

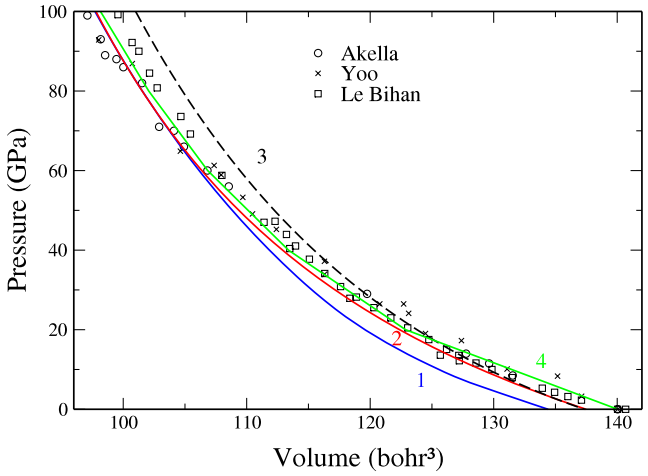

Figure 8. Comparison between experimental (○) [9], (×) [10], (□) [8] and theoretical 0 K isotherms for U calculated by us [11–13] [MTO bcc $l_{max} = 3$ (1), FPLAPW bcc (2), FPLAPW α-U (3)] or Li and Wang [14] [FPLAPW α-U (4)] in the bcc and α-U crystal structures.

high densities, and the ideal gas law, at high temperatures and low densities.

For the Debye temperature at ambient conditions we have taken $\theta_0 = 222$ K [5] and for the Grüneisen constant $\gamma_0 = 2.32$ [6]. For the Grüneisen function we use the simple empirical expression:

$$\gamma = \gamma_0 \frac{\rho}{\rho_0} + \frac{2}{3}\left(1 - \frac{\rho}{\rho_0}\right). \tag{26}$$

3.3. Cold curve

In the tension region ($\rho \leqslant \rho_0$) we use a semi-empirical expression provided by Panda:

$$E_c(\rho) = a_1 \exp(-a_2/\rho^{1/3}) - a_3\rho^{a_4} + E_b \tag{27}$$

E_b is the cohesive energy of the solid which is 2.20 MJ kg^{-1} for U [7]. The constants a_1, a_2 and a_3 are determined by the choices of E_b, of the equilibrium density and the bulk modulus at 0 K. The values have been chosen so that the density and the bulk modulus at ambient condition should be 19 g cm^{-3} and 104 GPa [8]. The constant a_4 has been fixed to 4 for a good agreement with the cold curve in the compression region.

In the compression region ($\rho \geqslant \rho_0$) the cold curve has been determined theoretically using two band calculation methods, the muffin tin orbital method (MTO) [11, 12] and the full potential linearized augmented plane wave method (FPLAPW) [13, 14]. The calculations with the MTO method have been done in the body-centered crystal structure (bcc) with expansions of the basis set to $l_{max} = 3$ (f states), while the calculations with FPLAPW have been done in the bcc and α-U crystal structures.

In figure 8 we can see that at low pressures the results with FPLAPW are better, but from 60 GPa the differences are small. In contrast, it is easier with the MTO method to do calculations at very high pressures when the conduction band mixes with the semi-core states 6s, $6p_{1/2}$, $6p_{3/2}$ and after with the $5d_{3/2}$, $5d_{5/2}$ states. Then the choices of the linearization energies in FPLAPW become difficult.

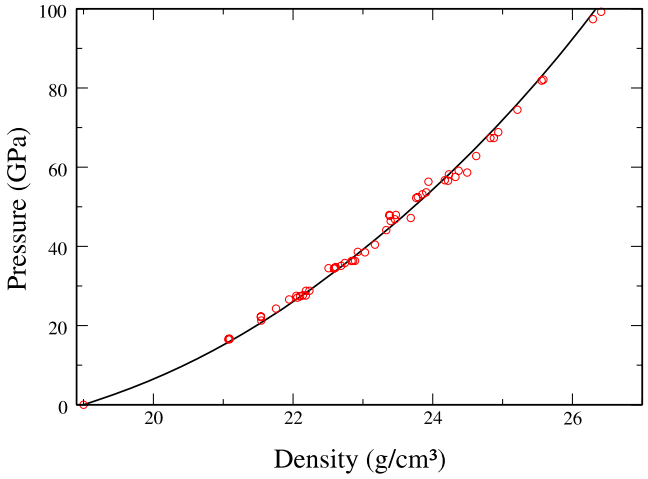

Figure 9. Comparison of the theoretical U Hugoniot with experiments (○) [15].

3.4. Hugoniot calculations

The thermodynamic properties, pressure P, energy E and density ρ of a compressed substance behind a shock front are determined from those of the initial state and from the shock wave parameters, shock velocity and particle velocity, according to the Rankine–Hugoniot relations [15]:

$$E - E_0 = 1/2\,(P + P_0)(1/\rho_o - 1/\rho). \tag{28}$$

A theoretical calculation of (28) requires the global EOS (1).

In figure 9, our theoretical Hugoniot is in very good agreement with the experimental points [15], but in this pressure range the effects of the thermal electronic contribution to the EOS is small. We could show higher pressures for Al.

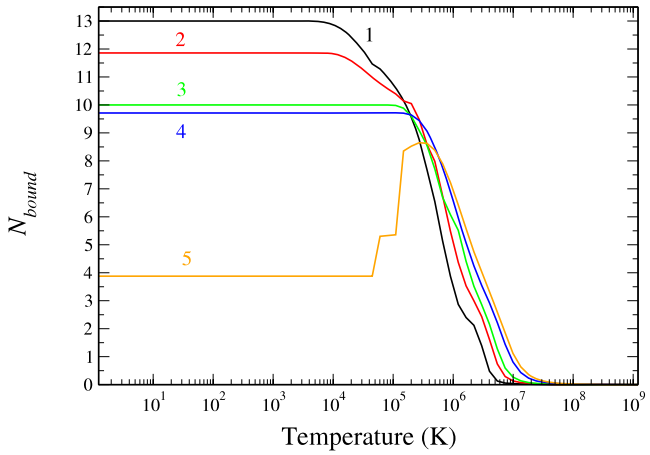

Figure 10. Number of bound electrons N_{bound} versus temperature for Al, for isochores 0.0495 (1), 0.774 (2), 2.7 (3), 19.9 (4) and 32.89 g cm^{-3} (5).

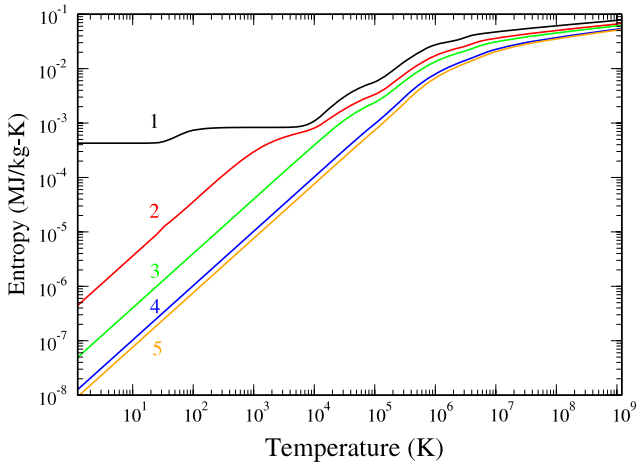

Figure 11. Entropy S_e versus temperature for Al, for isochores 0.0495 (1), 0.774 (2), 2.7 (3), 19.9 (4) and 32.89 g cm^{-3} (5).

4. Equation of state for aluminum

Our global EOS for Al has been built like U with the Panda code.

4.1. Thermal electronic terms

In figure 10 we show some isochores for N_{bound}.

For 0.0495 g cm^{-3}, at low temperature, there is no free electron, Al is in the free atom configuration; $1s^2 2s^2 3s^2 2p^6 3p^1$. At the higher density of 0.774 g cm^{-3}, at low temperature, Al becomes metallic; the Fermi level is in the continuum.

For 32.89 g cm^{-3}, at low temperature, the electronic configuration is $1s^2 2s^2$ plus about nine free electrons. When the temperature increases the $2p_{1/2}$ and after the $2p_{3/2}$ states appear and therefore the number of bound electrons increases. This number decreases at higher temperatures with the growing number of free electrons which are more energetic.

In figure 11 we can see no discontinuity on the isochore for entropy at 32.89 g cm^{-3} because, when the states $2p_{3/2}$ and $2p_{1/2}$ disappear at low temperature, they appear as resonances in the continuum. Then their global contribution to the entropy varies smoothly.

In figure 12 a comparison is done for the density 0.774 g cm^{-3} between entropies calculated by Paradisio or TF. We can see differences until 10^6 K.

4.2. Thermal ionic terms and cold curve

For the thermal ionic terms the same model used for U has been taken, with $\theta_0 = 383$ K [16] and $\gamma_0 = 2.16$ [16].

For the cold curve, in the tension region ($\rho \leqslant \rho_0$), where $\rho_0 = 2.7$ g cm^{-3} is the normal density, we also use (27) with $E_b = 12.25$ MJ kg^{-1} [16] and $B_0 = 73$ GPa [7].

In the compression region ($\rho \geqslant \rho_0$) we use the results which were obtained by band calculations with the APW (augmented plane waves) method [17].

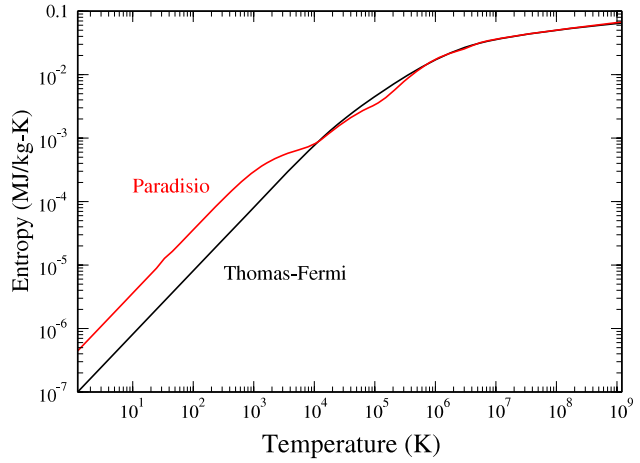

Figure 12. Comparison of entropies S_e calculated by Paradisio or TF at 0.774 g cm^{-3} for Al.

4.3. Results in the expanded region

In figure 13 we show our isotherms in the expanded region and we observe the same phenomena as seen in [16]. In going to small densities there is a first-order phase transition from the metallic dense phase (DP) to a nonmetallic DP before the transition nonmetallic DP–vapor. On the isotherm 9000 K there is therefore two stages of constant pressure corresponding to the two transitions. There are also two critical points at the top of the two curves which limit the coexistence regions, metallic DP–nonmetallic DP and nonmetallic DP–vapor.

Three phase transitions are now possible from the vapor to the nonmetallic DP, from the nonmetallic to the metallic DP, and from the vapor directly to the metallic DP (on isotherm 5000 K).

For the critical point metallic DP–nonmetallic DP, we have $T_{c2} = 11\,997$ K, $\rho_{c2} = 0.77$ g cm^{-3} and $P_{c2} = 2.86$ GPa.

For the critical point nonmetallic DP–vapor we have $T_{c1} = 11\,121$ K, $\rho_{c1} = 0.22$ g cm^{-3} and $P_{c1} = 0.435$ GPa.

The nonmetallic DP–metallic DP transition at low temperature happens when the free atom is compressed to

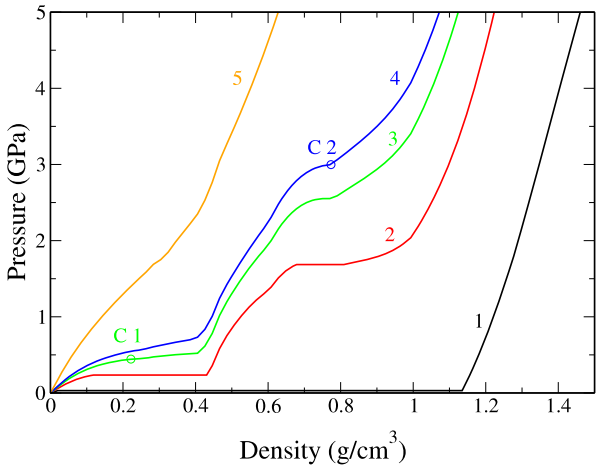

Figure 13. Isotherms [5000 (1), 9000 (2), 11 239 (3) 12 354 (4), 20 000 K (5)] in the expansion region with Maxwell constructions for Al. The thermal electronic contribution is calculated with Paradisio and there are two critical points: metallic dense phase (DP)–nonmetallic DP (C 2) and nonmetallic DP–vapor (C 1).

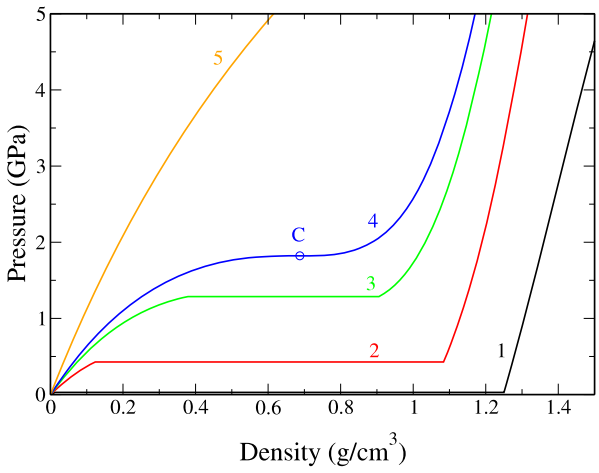

Figure 14. Isotherms [5000 (1), 9000 (2), 12 000 (3) 13 214 (4), 20 000 K (5)] in the expansion region with Maxwell constructions for Al. The thermal electronic contribution is calculated with TF. There is only one critical point (C).

about 0.77 g cm^{-3} where 1 electron of the 3p^1 state and 0.15 electrons of the 3s state pass into the continuum.

Because the original Inferno code was incorrect in the low-density region, as demonstrated in [2], in [16] the thermal electronic entropy at low density was obtained through an ionization equilibrium theory connected to the results of the original Inferno code [1] at higher densities.

We obtain a good value of 2505 K for the boiling point under atmospheric pressure: the experimental value is 2333 K [7].

In figure 14 we show the isotherms in the expanded region when the thermal electronic terms are calculated with TF instead of Paradisio; the thermal ionic terms and cold curve are kept unchanged.

We observe few differences until 5000 K. We obtain almost the same value of 2462 K for the boiling point under atmospheric pressure.

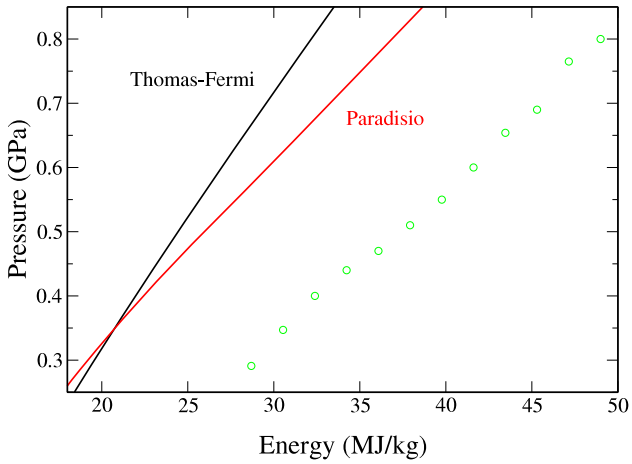

Figure 15. Pressure of Al at a density of 0.1 g cm^{-3} as a function of internal energy variation. The thermal electronic contribution is calculated with Paradisio or TF. Experiments (○) are from [18].

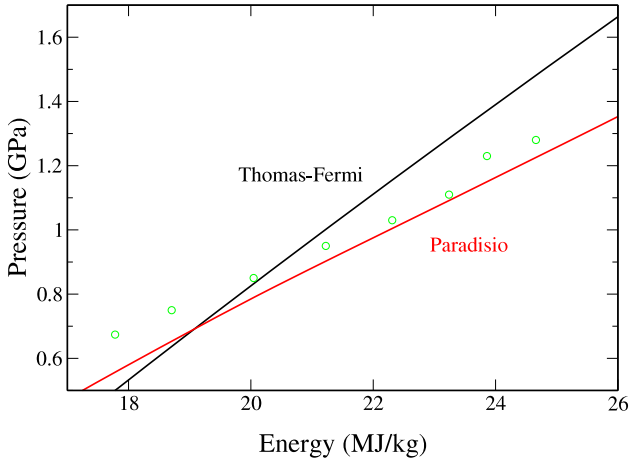

Figure 16. Pressure of Al at a density of 0.3 g cm^{-3} as a function of internal energy variation. The thermal electronic contribution is calculated with Paradisio or TF. Experiments (○) are from [18].

At higher temperatures, only the classical transition DP–vapor remains with the critical point $T_c = 13\,214$ K, $\rho_c = 0.69$ g cm^{-3} and $P_c = 1.82$ GPa.

We still observe differences at 20 000 K between TF and Paradisio.

Experimental measurements in the region of low densities and medium temperatures have been done [18]. Although the model we use to describe the liquid is very rough we can show the differences obtained when the thermal electronic term is calculated with Paradisio or with TF. Better models for the liquid could be tested in the future [16].

In figures 15 and 16 the differences that we see on the isochores 0.1 and 0.3 g cm^{-3} between Paradisio, TF and the experimental points are similar to the ones obtained with the Purgatorio code [2].

The lowest pressures in figures 15 and 16 correspond to temperatures greater than the ones in the phase transitions shown in figures 13 and 14.

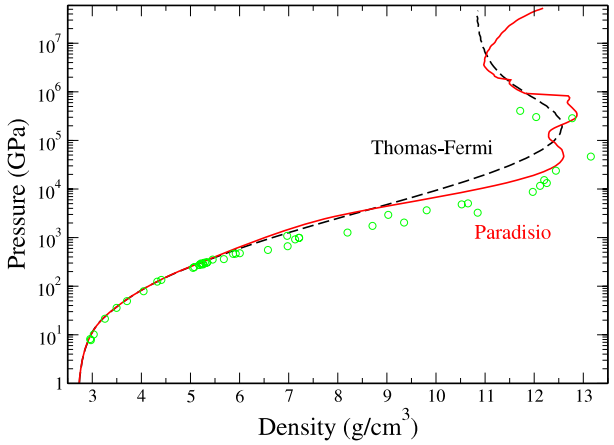

Figure 17. Comparison of the theoretical Al Hugoniots with experiments (○) [19]. The thermal electronic contribution is calculated with Paradisio or TF.

4.4. Hugoniot calculations

In figure 17 we compare the theoretical Hugoniots (28), obtained with a thermal electronic contribution from Paradisio or TF, with the experimental points [19]. Again the result is similar to the same comparisons done with the Purgatorio code [2].

The atomic structure effects included in Paradisio give higher compressions and a Hugoniot structure which cannot be obtained with TF. Furthermore, the Paradisio Hugoniot correctly goes to the relativistic limit of $7\rho_0$ (ρ_0 initial density) instead of $4\rho_0$ for our nonrelativistic TF.

5. Conclusions

To obtain the global EOS of warm matter we have presented an average atom code. The difficulty was that we want a model which gives a realistic answer for a huge domain of densities and temperatures. We have employed Liberman's relativistic and quantum model of matter which is a significant advance in complexity beyond the commonly used TF.

But the original code of Liberman, Inferno [1], employs approximations which limit its range of validity. In the same spirit of the Purgatorio code [2], but with different numerical procedures, we have found ways to deal with the resonant states in the continuum and the highly oscillatory nature of free wavefunctions at high temperatures until they can be approximated by ideal wavefunctions of an electron gas.

By adding to the thermal electronic terms, the thermal ionic terms and the cold curve, we have obtained a global EOS for U and Al in good agreement with experiment. In Al noticeable differences with TF have been shown. A shell structure appears on the high pressure Hugoniot and a first-order metallic–nonmetallic transition is created at low densities and temperatures.

References

[1] Liberman D A 1979 *Phys. Rev.* B **20** 4981
[2] Wilson B, Sonnad V, Sterne P and Isaacs W 2006 *J. Quant. Spectrosc. Radiat. Transfer* **99** 658
[3] Abramowitz M and Stegun I A 1970 *Handbook of Mathematical Functions* (New York: Dover)
[4] Kerley G I 1981 User's Manual for Panda: A Computer Code for Calculating Equations of State *Los Alamos National Laboratory Report, LA-8833-M* unpublished
[5] Flotow H E and Osborne D W 1966 *Phys. Rev.* **151** 564
[6] Steinberg D J 1976 Determination of the Grüneisen thermodynamic lattice gamma for α-plutonium *Lawrence Livermore Laboratory Report, UCDI-17033* unpublished
[7] Gschneider K A 1964 Physical properties and interrelationships of metallic and semimetallic elements *Solid State Physics* vol 16, ed H Ehrenreich, F Seitz and D Turnbull (New York: Academic)
[8] Le Bihan T, Heathman S, Idiri M, Lander G H, Wills J M, Lawson A C and Lindbaum A 2003 *Phys. Rev.* B **67** 134102
[9] Akella J, Smith G S, Grover R, Wu Y and Martin S 1990 *High Pressure Res.* **2** 295
[10] Yoo C S, Cynn H and Söderlind P 1998 *Phys. Rev.* B **57** 10359
[11] Pénicaud M 1984 *Shock Waves in Condensed Matter 1983* ed J R Asay, R A Graham and G K Straub (Amsterdam: Elsevier) p 61
[12] Pénicaud M 1997 *J. Phys.: Condens. Matter* **9** 6341
[13] Pénicaud M 2002 *J. Phys.: Condens. Matter* **14** 3575
[14] Li L and Wang Y 2001 *Phys. Rev.* B **63** 245108
[15] Marsh S P 1980 *LASL Shock Hugoniot Data* University of California, Berkeley
[16] Kerley G I 1987 *Int. J. Impact Eng.* **5** 441
[17] McMahan A K and Ross M 1979 *High Pressure Science and Technology* ed K Timmerhaus and M S Barber (New York: Plenum)
[18] Renaudin P, Blancard C, Clérouin J, Faussurier G, Noiret P and Recoules V 2003 *Phys. Rev. Lett.* **91** 75002
[19] Bushman A V, Lomonosov I V and Khishchenko K V *Shock Wave Database* http://teos.ficp.ac.ru/rusbank